Article

Not peer-reviewed version

Non-Tumorigenic Mesangiogenic Progenitor Cells (MPCs) Spontaneously Form Vascularized Xenografts in Athymic Nude Mice

Simone Pacini *, Marina Montali, Paolo Domenico Parchi, Paola Orlandi, Serena Barachini, Enza Polizzi, Angela Pucci, Guido Bocci

Posted Date: 28 April 2026

doi: 10.20944/preprints202604.1955.v1

Keywords: mesangiogenic progenitor cells; *Oct-4*; *Sox15*; Nanog; tumorigenicity; cartilage; tissue repair; cell-based medicinal product; CD34; nestin

 doi:10.20944/preprints202604.1955.v1

Article

Non-Tumorigenic Mesangiogenic Progenitor Cells (MPCs) Spontaneously Form Vascularized Xenografts in Athymic Nude Mice

Simone Pacini [1,*], Marina Montali [1], Paolo Domenico Parchi [2], Paola Orlandi [1], Serena Barachini [1], Enza Polizzi [1], Angela Pucci [3] and Guido Bocci [4]

[1] Department of Clinical and Experimental Medicine, University of Pisa, Pisa, Italy
[2] Department of Surgical, Medical and Molecular Pathology and Critical Care Medicine, University of Pisa, Pisa, Italy
[3] Histopathology Department, Pisa University Hospital
[4] Department of Translational Research and New Technologies in Medicine and Surgery, School of Medicine, University of Pisa, Pisa, Italy
* Correspondence: simone.pacini@unipi.it; Tel.: +39 050 993019

Highlights

What are the main findings?

- MPCs are mesengenic and vasculogenic cells isolated in human bone marrow cultures, this plasticity is supported by "adult" *Oct-4* circuit involving *Sox15*, *Nanog* and *Sall-4*. However, MPCs are not tumorigenic
- MPCs rapidly form vascularized xenografts that spontaneously undergoes dynamic changes in tissue architecture leading to a non-vascularized tissue sustained by a dense collagen fiber network.

What is the implication of the main finding?

- Despite expressing pluripotency-associated genes, MPCs can be considered intrinsically "non-tumorigenic," paving the way for the development of MPC-based medicinal products.
- MPCs could represent a new promise in cell therapy for musculoskeletal tissue repair, following the disappointing results obtained with MSCs.

Abstract

Background: Mesangiogenic Progenitor cells (MPCs) were first described in 2008 in cultures of human bone marrow mononuclear cells (hBM-MNCs) aimed at isolating mesenchymal stromal cells (MSCs) using human autologous serum. A selective culture method was subsequently developed to isolate MPCs with a high degree of purity, yielding approximately 1% of the total plated cells. Since their initial description, MPCs have demonstrated the ability to differentiate into highly clonogenic MSCs while retaining early vasculogenic potential. Gene expression profiling of MPCs revealed constitutive expression of pluripotency-associated transcription factors such as OCT-4 and NANOG, as well as SOX15 instead of SOX2, suggesting a possible molecular mechanism that sustains MPC plasticity, defined as the "adult *Oct-4* circuit". Although the expression of these pluripotency-associated markers has been hypothesized to represent a distinctive adult molecular circuit, concerns regarding the tumorigenic potential of MPCs are reasonable and have not yet explored. *Methods*: Here, we present data from the tumorigenicity test in partial compliance with WHO recommendations of two different MPC-derived cell products in athymic nude mice. *Results*: Histomorphometric analysis of nodules excised from animals at 6, 8, or 12 weeks post-cell transplantation excluded tumor formation and demonstrated the ability of MPCs to generate homogeneous and organized tissue through distinct phases: an "*early*" vasculogenic phase, followed by remodeling of the newly formed microvascular network and the deposition of structured, aligned collagen fibers. *Conclusions*: MPCs

 doi:10.20944/preprints202604.1955.v1

do not possess intrinsic tumorigenic potential and spontaneously form vascularized xenogenic tissue four weeks after injection into the subcutaneous space.

Keywords: mesangiogenic progenitor cells; *Oct-4*; *Sox15*; Nanog; tumorigenicity; cartilage; tissue repair; cell-based medicinal product; CD34; nestin

1. Introduction

Mesangiogenic progenitor cells (MPCs) were first identified in human bone marrow mononuclear cell (hBM-MNC) cultures using autologous serum as a supplement instead of bovine serum [1]. Subsequently, a cheap and reliable method was developed to produce MPCs at a very high purity grade (>95%) in just 3 to 5 days of culture [2] From the beginning, MPCs attracted particular attention for their ability to efficiently differentiate into exponentially growing mesenchymal stromal cells (MSCs) [3], while retaining a genuine vasculogenic potential both in vitro and in vivo, although these two cell fates have been shown being mutually exclusive [4]. Moreover, it has been demonstrated that, in vitro, both mesengenic and vasculogenic MPC differentiation pathways proceed through an intermediate state of differentiation. Indeed, MPCs should first differentiate into MSCs to obtain intracellular lipid accumulation or extracellular calcium deposition [3], similarly inducing endothelial sprouting from 3D-spheroids is mandatory to obtain vasculogenic cells [4].

After the discovery of the in vivo progenitor of MPCs [5], it was possible to compare their ex vivo frequency estimated by flow cytometry, ranging from 0.5 to 3.0% of total hBM-MNCs, with the frequency of MPCs estimated after isolation under selective culture conditions, ranging from 1.0 to 3.5% of plated mononuclear cells. Additionally, it was possible to evaluate yield and recovery during the MPC production. Conclusions from this comparison were; (i) MPC and their ancestor were found to be 1'000 to 10'000 times more frequent than mesenchymal stromal cells (MSCs) in hBM-MNCs [2], (ii) MPCs do not proliferate during the isolating procedure, as reported in 2009 and confirmed by Ki-67 negative stain [1], and (iii) it is possible to obtain 1 to 3 million MPCs from 5-10 ml of BM aspirate after a few days of culture.

Alongside its potential clinical value in determining the efficacy of the cell-based medicinal product (CBMP), the possible application of cell products containing highly purified MPCs could also offer significant advantages to consider during risk assessment. Since MPCs have been shown to maintain a quiescent state, during a very short-term isolation procedures, the safety of their possible clinical application could benefit from a: (i) a reduced risk of cell transformation and genomic instability, (ii) a decreased cellular senescence, and (iii) a reduced exposition to bacterial and viral contamination, minimizing culture time to 3-5 days [6]. Nonetheless, pre-clinical studies investigating the safety of CBMP containing highly purified MPCs from hBM-MNCs, have not been conducted yet.

In addition to affordable methods for isolating these cells, the retention of both mesengenic and vasculogenic potential makes MPCs a promising tool in tissue repair and regenerative medicine, particularly for regenerating poorly vascularized musculoskeletal tissues such as degenerated articular cartilage or critical bone defects with non-union fracture ends [7]. In this context, pre-implantation MPC vasculogenic differentiation could significantly improve survival and regeneration in such hostile microenvironments.

In the field of cell therapy and tissue regeneration, among various key safety concerns, the risk of tumor formation attributable to cell administration, has become central particularly in the recent years as promising new CBMPs derived from human pluripotent stem cells (hPSCs) have been proposed for clinical use [8].

MPCs are adult somatic cells; however, they possess longer telomeres compared to freshly isolated hBM-MSCs, and also express pluripotency-associated markers, including: *octamer-binding transcription factor* 4 (*Oct-4*), *SRY-box transcription factor 15* (*Sox15*) and *Nanog* [9]. Although it has been hypothesized an "adult" *Oct-4* activity for MPCs, involving the homodimer and the heterodimer *Oct-*

 doi:10.20944/preprints202604.1955.v1

4/*Sox15* instead of the stemness-related heterodimer *Oct-4*/*Sox2*, concerns about the tumorigenic potential of MPCs are reasonable.

The World Health Organization (WHO) defines tumorigenicity as "*the capacity of a cell population inoculated into an animal model to produce a tumor by proliferation at the site of inoculation and/or at a distant site by metastasis*" [10]. Based on this definition, the conventional approach for testing tumorigenicity is primarily implanting the cell product at an ectopic site, such as subcutaneously or under kidney capsule, in immunodeficient mice and monitoring for the formation of tumor masses [11].

Thus, to test the intrinsic tumorigenicity of MPCs, we performed subcutaneous inoculation of freshly isolated MPCs in six-week-old Athymic Nude-Foxn1^{nu} (CD *nu*/*nu*) male mice. In addition, sprouted MPC 3D-spheroids were also inoculated to determine whether in vitro pre-implantation vasculogenic differentiation influences MPC fate in vivo. Both cell types were obtained through pre-implantation induction under controlled and well-characterized in vitro specific culture conditions. Taking into consideration the above-mentioned fact that most MPC features were lost after mesengenic differentiation [3,4], the subcutaneous implantations were replicated using exponentially growing MSCs derived from MPC mesengenic differentiation. Subcutaneous mass formation was monitored macroscopically for 12 weeks, after which the animals were sacrificed to allow microscopic evaluation of the injection site. Notably, because data from the initial experiments revealed interesting xenograft tissue architecture, the experimental design was expanded to include sacrifices at 4, 6, and 8 weeks after cell injection to monitor xenogenic tissue formation.

2. Materials and Methods

2.1. Human Bone Marrow Collection and Mononuclear Cell Isolation

After obtaining written informed consent, hBM aspirates were collected from 20 donors (12M/8F, median age: 68, range 52-85) undergoing orthopedic surgery for hip replacement. Briefly, a 20-mL syringe containing 500 I.U. of heparin was used to aspirate 10 mL of fresh bone marrow immediately after femoral neck osteotomy and during femoral reaming. Fresh bone marrow samples were diluted 1:4 in Dulbecco's modified phosphate-buffered saline (D-PBS; Thermo Fisher, Waltham, MA-USA) and gently layered onto Ficoll-PaqueTM PREMIUM (GE Healthcare, Uppsala, Sweden). Samples were centrifuged at 400g for 25 min and mononuclear cells (hBM-MNCs) were collected at the interface, filtered through 70 μm filters, and washed twice with D-PBS. For quality control, 2x10^4 cells were processed for immuno-phenotyping to quantify the *Pop#8* population, according to [5] and hemodilution was assessed according to [12].

2.2. Mesangiogenic Progenitor Cells (MPCs) Isolation

According to [2], hBM-MNCs were plated at a density of 8 × 10^5/cm^2 in hydrophobic T-75 flasks (GreinerBio-One, Kremsmünster, Austria) and cultured in low-glucose Dulbecco's modified Eagle medium (DMEM, Thermo Fisher) supplemented with 10% pooled human AB type serum (PhABS, Lonza, Walkersville, MD-USA), 2 mM Glutamax® (Thermo Fisher), 100 μg/mL gentamicin (Thermo Fisher). Culture medium was completely replaced every 48h. After 4–6 days, plates were morphologically screened for MPCs using an inverted microscope. Cells were then detached by TrypLE Select® (Thermo Fisher) digestion and washed in D-PBS. A total of 2x10^4 cells were processed for immuno-phenotyping to evaluate the purity of the cell product.

2.3. Obtaining MPC-Derived Mesenchymal Stromal Cells (MSCs)

Freshly detached MPCs obtained as described above were seeded at 2x10^4 cells/cm^2 in TC-treated T75 flasks and allowed to adhere in DMEM/10% PhABS. After 24 h medium was replaced with StemMACS™ MSC Expansion Media XF (Miltenyi Biotec) and cultures were grown to confluence to obtain passage one MSCs (P1-MSCs). Cells were then detached using TrypLE Select® and subcultured at a 1:2 ratio to confluence to obtain passage two MSCs (P2-MSCs). A total 2x10^4 cells were processed for immuno-phenotyping to confirm the MSC phenotype and to exclude the

 doi:10.20944/preprints202604.1955.v1

presence of residual MPCs. In parallel, 1x10^5 cells were plated in two TC-treated 6-wells and cultured 48h in StemMACS™ MSC Expansion Media XF. Medium was then replaced with StemMACS™ OsteoDiff Media or StemMACS™ AdipoDiff Media (Miltenyi Biotec) and cultures were maintained for at least two weeks. Cultures were stained with Alizarin-S to detect calcium deposition or with Nile Red fluorescent dye to detect lipid droplets.

2.4. Flow Cytometry

Freshly detached cells (200,000 cells per sample) from MPC or P2-MSC cultures were washed twice with MACS Quant® Running Buffer (Miltenyi Biotec, Bergisch Gladbach, Germany) and incubated with anti-human CD90 FITC-conjugated, CD73 PE-conjugated, CD31 PE/Cy7-conjugated, CD14 VioGreen®-conjugated, and CD45 VioBlue®-conjugated antibodies (Miltenyi Biotec) for 30' at 4 °C in the dark. Data were acquired using a MACS Quant® flow cytometer and analyzed with MACS Quantify® Analysis Software (Miltenyi Biotec). Cellular events were selected using a light scatter plot (SSC vs. FSC), excluding low scatter signals. Plotting forward scatter signals as peak height *versus* area (FSC-H vs. FSC-A) allowed for the selection of singlet events. The purity of MPC cultures was then calculated as the number of CD31$^+$CD90^{neg} events relative to the total number of cellular singlet events. Similarly, the purity of P2-MSC cultures was calculated as the number of CD90$^+$ events relative to the total number of cellular singlet events.

2.5. 3D Spheroids Preparation and Sprouting Induction

3D spheroids (6 to 8 per experiment) were prepared using the hanging drop method, applying 1.5x10^5 cells/drop, as previously described [4] applying freshly detached MPCs or P2-MSCs as "no sprouting control". The following day, 3D spheroids were gently transferred onto a thick layer of Geltrex™ LDEV-Free reduced growth factor basement membrane Matrix (Thermo Fisher) and cultured in EGM-2 medium (Lonza) for a week, medium was replaced every 48h. At the end of the culture period, the medium was removed and plates were incubated on ice for 20' to liquefy the gel. An 18-gauge needle was attached to a syringe to collect the spheroids while preventing their dissociation.

2.6. Subcutaneous Implantation in Nude Mice and Clinical Observation

Six-week-old Athymic Nude-Foxn1^{nu} (CD nu/nu) male mice supplied by Envigo (Milan, Italy), were housed in micro-isolator cages on vented racks. They were handled using aseptic techniques, and were allowed unrestricted access to sterile food and water.

Each experiment employed the minimum number of mice necessary to obtain statistically meaningful results. Nude mice, weighing 25 g were anesthetized with a 1:1 combination of tiletamine and zolazepam (Zoletil®), 50 mg/kg, administered intraperitoneally before the inoculation procedure. On day 0, mice were inoculated subcutaneously into the rear supraclavicular region of the trunk using an insulin syringe with a 0.5x16-mm needle. Animals were monitored for 24 hours following the treatment.

A total of twenty mice received a single injection of 300 µl vehicle (Geltrex™) alone and the inoculation of one of the four different cell constructs, each prepared by adding 300 µl of Geltrex™ to: (group *A*) 1.5 to 2.0x10^6 MPCs (n=8); (group *B*) 8 to 10 MPC 3D spheroids (n=8); (group *C*) 1.5 to 2.0x10^6 MPC-derived MSCs (n=2) and (group *D*) 8 to 10 MSC 3D spheroids (n=2).

All animals were observed once or twice daily for mortality, moribundity, and general appearance. Additionally, animals were inspected for growing masses. Animals from groups *A* and *B* were euthanized by using an anesthetic overdose of zolazepam (Zoletil®) at 4, 6, 8 or 12 weeks post-implantation. Animals from groups *C* and *D* were sacrificed 12 weeks after cell transplants. Necropsy examinations were performed on the scheduled sacrificed animals. After exsanguination via the vena cava and aorta, the back was incised, and all skin layers were excised, separating subcutaneous fat from muscle tissue to expose the inoculation site. This allowed precise excision of the newly formed

 doi:10.20944/preprints202604.1955.v1

ectopic tissue for fixation in 10% (v/v) neutral buffered formalin. Additionally, all animals were examined for external and internal abnormalities, and lungs, liver, spleen and kidneys were removed. Tissues were fixed for 48 hours, then transferred sequentially to 70% ethanol, 96% ethanol, absolute ethanol and Bio-Clear (Bio-Optica, Milan, Italy) at room temperature for one hour each. Fixed tissues were then embedded in paraffin wax.

2.7. Histological and Histomorphometric Analysis

Formalin-Fixed Paraffin-Embedded (FFPE) implants serial sections (5µm each) were prepared by Leica RM 2155 microtome (Leica Biosystems, Wetzlar, Germany) and gently mounted on Polysine® slides (Thermo Scientific, Waltham MA, USA). Standard hematoxylin/eosin (H&E) staining was performed every 20 sections throughout the series. Microscopic evaluation was conducted using a Leica DMR microscope (Leica Biosystems, Wetzlar, Germany) to identify the central median section (cmSec) of the series based on the extent of newly formed tissue. Pentachrome Russell-Movat staining, modified by Doello [13], was used to assess collagen fibers and sulfated mucopolysaccharides distribution. This staining was applied to the section immediately following the middle section (cmSec+1), cmSec+20 and to cmSec-20. In addition, to assess the presence of calcium deposits, the von Kossa staining was performed on cmSec+2, cmSec+21 and cmSec-21. Brightfield tile scans of the sections were performed using Leica SP8 microscope equipped with LAS X Navigator® software (Leica) producing a single mosaic image for each section. A specific image processing workflow in ImageJ software (NIH, Bethesda, Maryland, USA) was optimized to analyze pentachrome stain, resulting in three different binary images: osteoid-like (OstBin), adipose (AdipoBin) and collagen (CollBin) binary images of the xenograft from each mosaic. Briefly: i) to exclude murine skin tissue, a specific region of interest (ROI) was freehand drawn surrounding the ossicle (Supplemental Figure S1 A), ii) RGB histogram color thresholds were defined to detect tissue from the background and extract the OstBin image. Inverting this pixel selection generates background binary images. By applying specific histogram color threshold, mainly excluding most of the pixels in the green channel, it was possible to selectively identify the red color corresponding to the collagen fibers generating the CollBin image (Supplemental Figure S1 B). The background binary was then processed by particle analysis to specifically select only the rounded unstained lipid vacuoles generating the AdipoBin image (Supplemental Figure S1 C). iii) the total xenograft area (TotArea) was measured by adding the pixel^2 value from OstBin and AdipoBin and converted in μm^2 on calibrated images. The percentage of area fraction (%Area) for each binary was calculated on TotArea. The entire workflow described above was applied three times to a single mosaic image, and the mean values TotArea and %Area were recorded. Finally, the image analysis was validated if the calculated coefficient of variation (CV) among the three measurements was less than 2%. Statistical analysis was performed using one-way analysis of variance (ANOVA) followed by non-parametric Dunnett's post-test for multiple comparison.

For each histological sample, the whole xenograft area from cmSec+1, cmSec+20 and cmSec-20 were scored by three independent and skilled histopathologists, each with specialized experience in oncologic pathology. Pathologists were blinded to information regarding the origins of the nodule sections, and to each other's assessments. Xenografts slides were scored according to WHO criteria for grading soft tissue tumors [14]. Tumor grades were treated as categorical variables. For cases in which at least two out of three pathologists assigned the same tumor grade, this grade was accepted as the final reference standard (majority-rule consensus). Cases in which all three pathologists assigned different grades were submitted to an adjudication session. In addition, pathologists were asked to manually count the absolute number of vessels and microvessels and to quantify the Ki-67 proliferation index according to the International Ki-67 in Breast Cancer Working Group (IKWG) guidelines [15]. Vessel counts were recorded as median values calculated from three separate counts for each section analyzed. Vessel density (VD) was then calculated by dividing the median number of vessels by the OstBin area expressed in μm^2. Statistical analysis was performed using one-way analysis of variance (ANOVA) followed by parametric Dunnett's post-test for multiple comparison.

 doi:10.20944/preprints202604.1955.v1

Results are presented as mean value ± standard error (SE). Ki-67 proliferation index was assessed using the "global" method. Five fields, each containing 100 cells, were selected to capture the observed heterogeneity in nuclear staining, excluding areas with necrosis, vessels, or artifacts. Slides were classified as having a "low proliferation" index if the percentage of Ki-67-positive nuclei was ⩽1% [16].

3. Results

3.1.1. Characterization of Cell Products

Sixteen bone marrow samples were processed for the production of MPCs due to their very low peripheral blood contamination index (PBCI, -0.57 ± 0.38, n = 16) [12] and Pop#8 frequencies ranging from 1% to 2% (1.67 ± 0.54%; n = 16) as expected in human bone marrow [5]. Four samples showed a PBCI greater than 1.2 and were discarded. As expected, MPC isolation produced from 1.5 to over 3.0 x10^6 (1.93 ± 0.67 x 10^6, n = 16) cells from each samples. All MPCs products exhibited a high purity grade, characterized by the $CD31^{bright}CD14^{neg}CD90^{neg}CD73^{neg}$ phenotype, with percentages ranging from 96% to 98% (97.4 ± 0.8%, n = 16, Figure 1A). Efficient mesengenic differentiation toward exponentially growing P2-MSCs was achieved from all of the MPC preparations after culture in StemMACS™ MSC Expansion Media XF. The mesenchymal $CD31^{neg}CD14^{neg}CD90^{bright}CD73^{bright}$ phenotype was also confirmed by flow cytometry (Figure 1B) and differentiation potential was verified by detecting calcium deposition and lipid droplet accumulation under osteogenic and adipogenic stimuli, respectively (data not shown). 3D-spheroids were obtained from both MPCs (Figure 1C) and P2-MSCs (Figure 1D); however, as expected, only MPC-derived 3D-spheroids were able to sprout when cultured with EGM-2 medium.

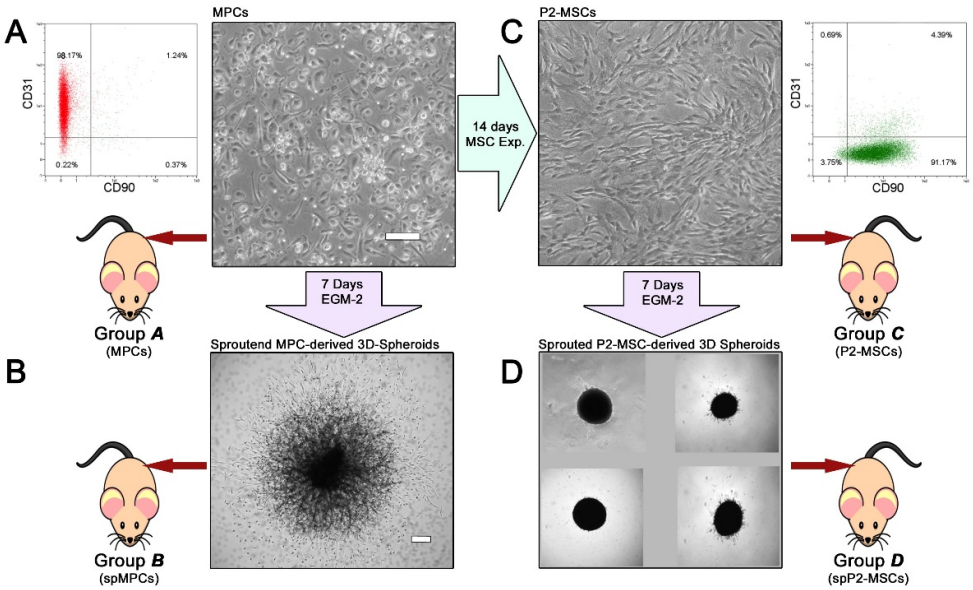

Figure 1. CharacFigure 1. *Characterization of cell products used for inoculation*. (A) Culturing hBM-MNCs in DMEM supplemented with 10% PhABS for 4–6 days resulted in a monomorphic adherent population of rounded, birefringent MPCs expressing CD31 but not CD90. Between 1.5 and 2.0 million MPCs were resuspended in Geltrex® and transplanted into mice from experimental group "*A*". (B) A portion of freshly detached MPCs was used to produce 3D spheroids. After 7 days of stimulation in EGM-2 medium, sprouting exceeding 300 µm from the spheroid edge was observed under an inverted microscope, confirming the preparation for inoculation in mice from experimental group "*B*". (C) Freshly detached MPCs were alternatively cultured for two passages in StemMACS™ MSC Expansion Medium obtaining $CD31^{neg}CD90^{+}$ P2-MSCs with typical spindle-shaped morphology; these cells were directly inoculated into mice from experimental group "*C*". (D) Expanded P2-

 doi:10.20944/preprints202604.1955.v1

MSCs were sufficient for both direct inoculation and 3D spheroid preparation. As expected, P2-MSC-derived spheroids did not exhibit sprouting and were inoculated into mice from experimental group "*D*" as "no sprouting control" 3D spheroids. Scale bars = 100 μm.

3.1.2. In Vivo Experiments

All animals from each experimental group survived until the scheduled necropsy date without any signs of morbidity or significant weight loss. External inspection before skin excision revealed small but palpable nodules at the cell injection site in all animals (Supplemental Figure S2A); however, the reduced size of the nodules hindered precise measurement. Conversely, the vehicle injection site was not identifiable in any treated animals, suggesting that the Geltrex™ was completely resorbed with no evidence of host reaction. Surgical dissection of the skin layers on the backs of all animals revealed no signs of tissue adhesion and allowed precise excision of the nodules for subsequent histological analysis (Supplemental Figure S2B). The excision of the vehicle injection site was guided by the marker placed on the day of Geltrex™ administration. These biopsies showed normal skin histology after both hematoxylin and eosin and Doello's pentachrome staining (Supplemental Figure S3).

3.1.3. Biopsy Analysis

Biopsies from group *A* mice, which received a suspension of MPCs, showed compact nodules without signs of encapsulation or any other host reaction (Figure 2). The xenogenic origin of the excised nodules was confirmed by positive immunofluorescent staining for the anti-human mitochondrial antigen, clone 113-1 (Supplemental Figure S4). Macroscopically, due to their small size and translucent appearance, precise evaluation of nodule size was difficult even after excision and was therefore performed during histomorphometric analysis. After revising the first few slides, a "calibration session" was necessary to adjust the WHO criteria for analyzing xenografts instead of tumor masses. The three pathologists agreed to limit grading assignments to cytological features such as; morphology, mitotic activity, Ki-67 proliferation index, differentiation level and invasion, while excluding the evaluation of tissue architectural features. Additionally, the pathologists agreed to include a grade "0," indicating cells that resemble normal cells with very rare or absent mitotic figures (Supplemental Figure S5), low proliferation index (⩽1% of Ki-67-positive cells, Supplemental Figure S6) and no invasion of surrounding tissue. Following the calibration session and the review of the entire series of slides stained with both hematoxylin/eosin and pentachrome, the three pathologists reached a consensus (3/3) on tumor grade "0," regardless of the time to sacrifice, rendering the "adjudication session" unnecessary.

In general, further comments from the pathologists highlighted the scarce cellularity and modest vascularization, with vessels of regular but small caliber, at 4 and 6 weeks from cell injection. Ki-67 proliferation index resulted very similar in all examined slides, and less than 1.0% of positive cells were detected (range 0.0-0.7%). Ki-67 positivity was observed in no cells or in exceptionally rare cells, besides endothelial cells of the accompanying vessels, no mitotic figure was detected in any case (Supplemental Figure S5).

Indeed, nodules consisted of a homogeneous, sparsely cellular tissue supported by a dense network of collagen fibers (stained scarlet red), which appeared to thicken over time. Notably, most cell nuclei were detected in close contact with collagen fibers. In the early phase of tissue formation, after four weeks, a dense and widely distributed vascular network, composed mainly of small or capillary-like perfused vessels, was also evident and showed positive staining for the anti-CD34 and anti-nestin antibody (Figure 4A). However, the number of these microvessels significantly decreased after eight weeks and disappeared entirely by twelve weeks. Nodules from group *B*, transplanted with sprouted 3D spheroids derived from MPCs, exhibited xenogenic tissue characterized by an inhomogeneous distribution of collagen-rich regions and different areas containing large lipid vacuoles while lacking any organized collagen fibers (Figure 3). Pathologists' revision assigned a unanimous consensus of grade "0" independently by the time to sacrifice and the histological

 doi:10.20944/preprints202604.1955.v1

characteristics of nodules from group *B* did not appear to change over time following cell transplantation. Perfused microvessels were detected but markedly lower numbers compared to group *A* samples; these vessels were found predominantly in close contact with lipid vacuoles. At higher magnification, differences in the newly formed microvascular bed became apparent between compact collagen-rich regions, also detected in group *B*, and fat-like regions of the xenogenic tissues (Figure 5). In particular, within the xenograft formed after the implantation of untouched MPCs most of the perfused microvessels exhibited a tubular appearance with a nearly uniform caliber, ranging from approximately 10 μm to no more than 80–100 μm. These vessels were associated with a thick basement membrane composed of collagen fibers (Figure 5 A) and were occasionally surrounded by perivascular cells (white arrow in Figure 5 A). Immonofluorescence revealed positive stains both for CD34 and nestin. (Figure 4 A). A similar morphology was also observed in the collagen-rich region of the excised nodules from group *B*. In contrast, microvessels found in close proximity to the numerous adipocytes within the newly formed fat-like tissue of group *B* (Figure 5 B) displayed a convoluted morphology with thin walls consisting of a single layer of flattened endothelial cells. These vessels lacked an associated basement membrane and perivascular cells (black arrow in Figure 4B) and resulted CD34-negative and nestin-negative (Figure 4 B).

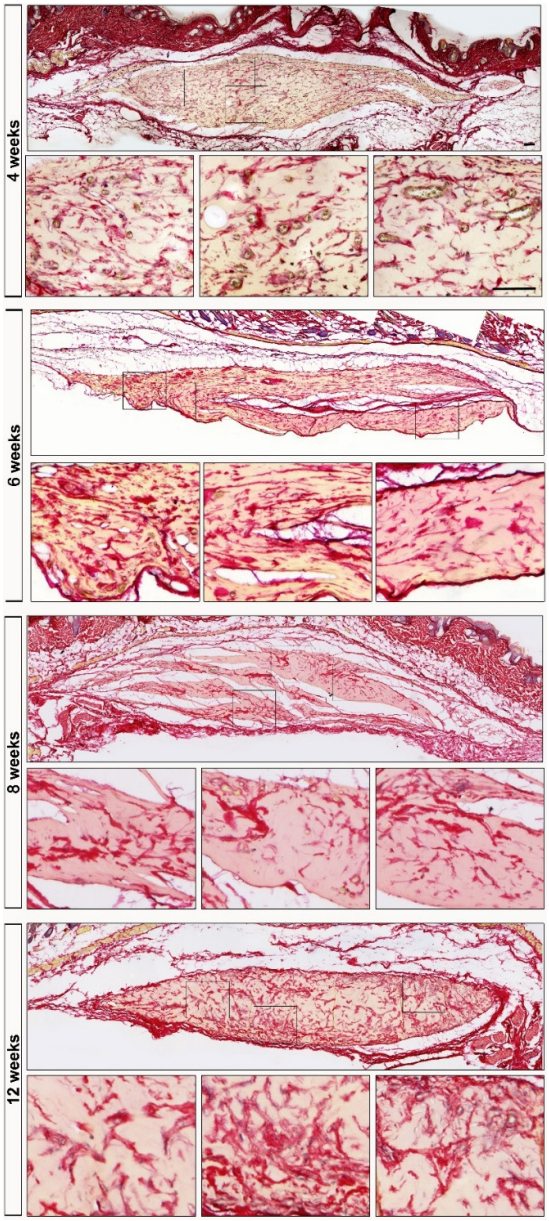

 doi:10.20944/preprints202604.1955.v1

Figure 2. *Pantachrome stain of the central median section +1 (cmSec+1) of excised nodules from group A mice*. Nodules excised from mice implanted with a suspension of MPC showed compact, poorly cellularized tissue (stained pale yellow, with cell nuclei stained purple) characterized by a dense network of collagen fibers (stained scarlet red), which thickened over time. Numerous perfused microvessels (erythrocytes stained yellow) were detected in the early phases of xenogenic tissue formation, but the tissue became non-vascularized after 12 weeks. Scale bars = 250 μm.

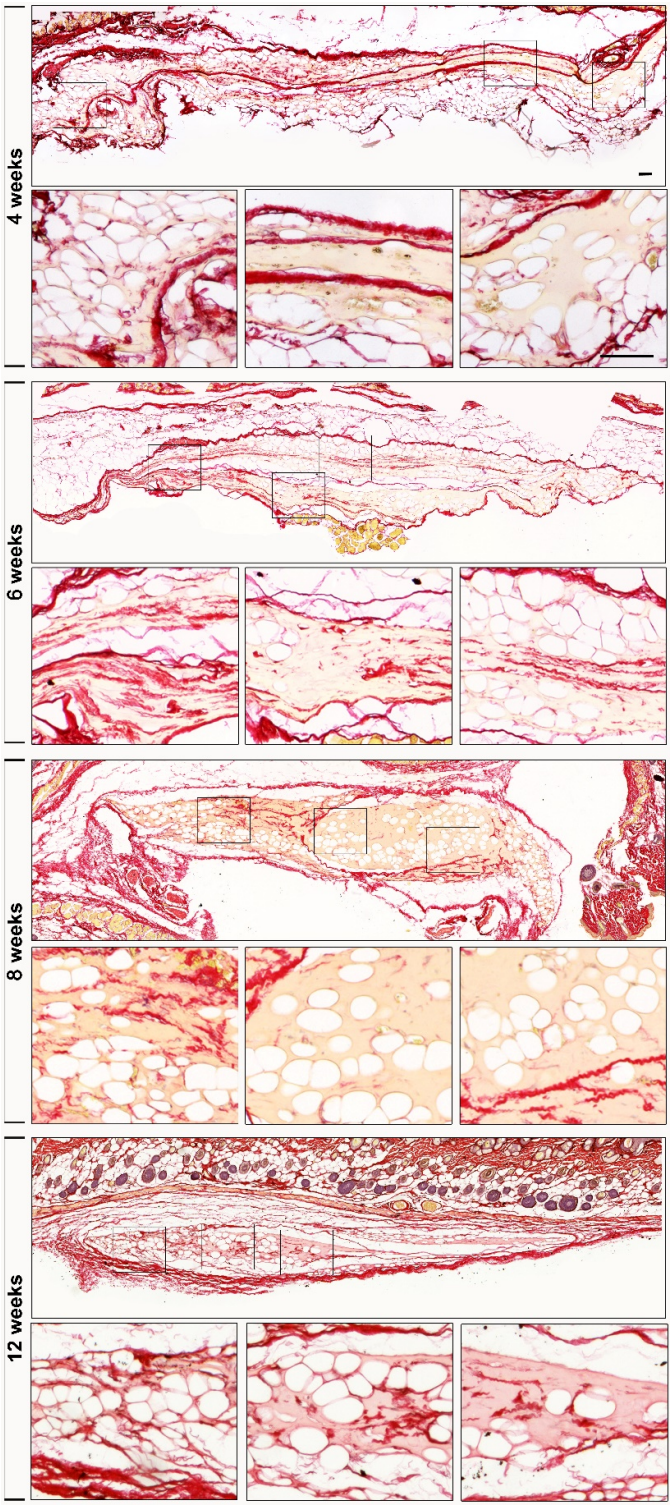

 doi:10.20944/preprints202604.1955.v1

Figure 3. *Pantachrome stain of the central median section +1 (cmSec+1) of excised nodules from group B mice*. Nodules excised from mice implanted with sprouted MPC 3D spheroids exhibited two distinct tissue organization patterns: a compact, sparsely cellular tissue characterized by a dense network of thick collagen fibers resembling the tissue observed in group *A*, alternating with areas containing numerous large mature adipocytes and lacking any collagen framework. Perfused, convoluted, thin-walled microvessels were frequently detected in close proximity to adipocytes, contrasting with the rounded, thick-walled microvessels found adjacent to collagen fibers in the osteoid regions. Scale bars = 250 μm.

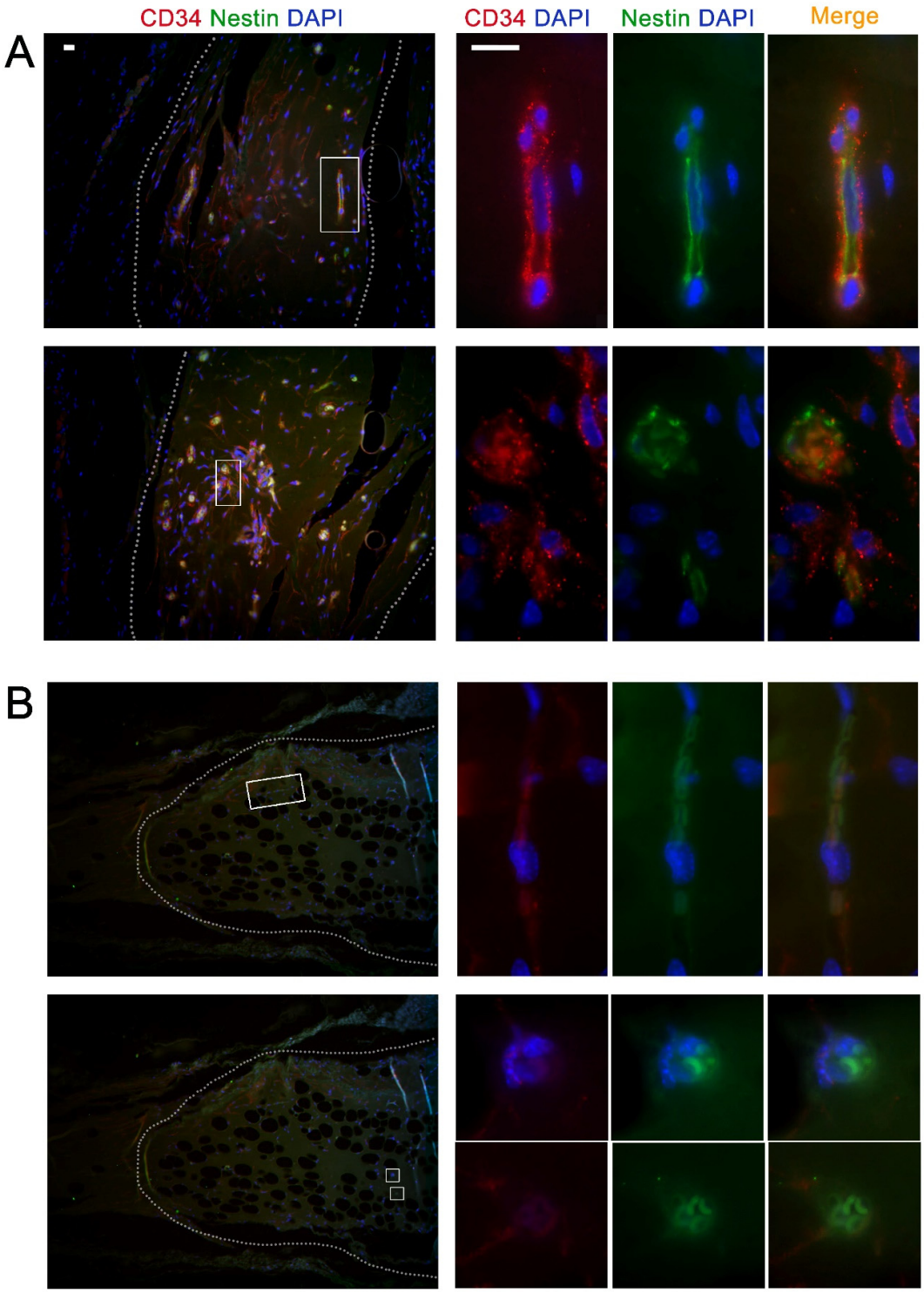

 doi:10.20944/preprints202604.1955.v1

Figure 4. *Co-occurrence of nestin and CD34 in newly formed, perfused microvessels within nodules from groups A and B mice.* (A) Representative images of sections from nodules of group *A* mice, formed after 4 weeks. Transverse and longitudinal sections of microvessels in the xenograft region (dotted lines) show expression of CD34 (red false color) and nestin (green false color) in endothelial cells (nuclei in blue false color). (B) Autofluorescence of erythrocytes enabled localization of perfused microvessels, which stained negatively for CD34 and nestin in the adipocyte-rich region (dotted lines) of nodules from group *B*, 4 weeks from cell injection. Scale bars = 20 μm.

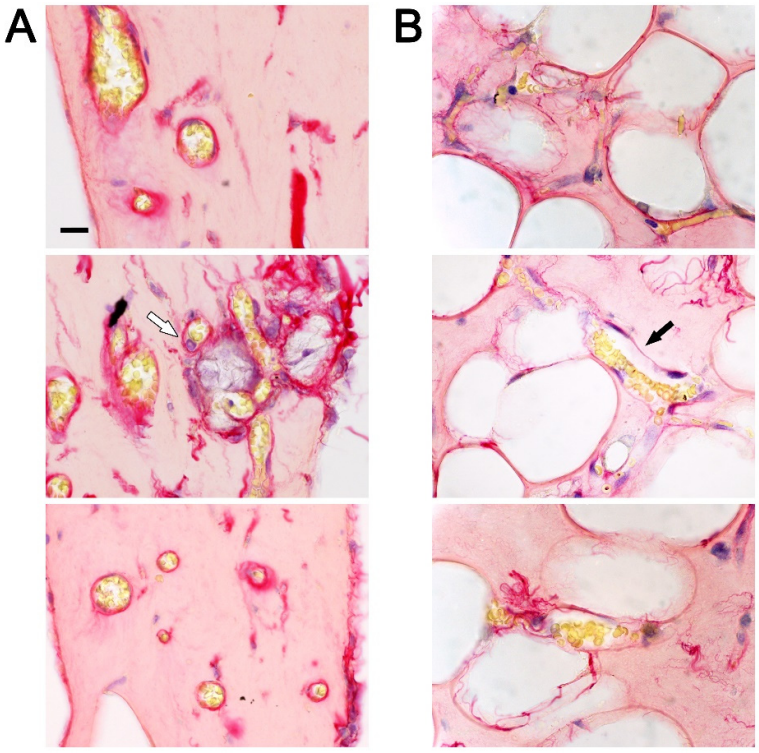

Figure 5. *Microanatomic differences in newly formed microvascular beds from xenogenic tissues excised from group A and B mice*. At higher magnification, (A) perfused microvessels detected in nodules from group *A* mice (receiving transplants of MPC in suspension) exhibited a tubular shape with a consistent caliber ranging from 1 to 8–10 erythrocyte diameters. A thick basement membrane was evident, surrounding the endothelial layer, and occasional accessory perivascular cells were detected (white arrow). (B) Conversely, perfused microvessels detected in nodules from group B mice (receiving transplants of sprouted 3D spheroids) showed thin walls consisting of a single layer of flattened endothelial cells, basement membrane matrix, and no perivascular cells (black arrow). Scale bar = 20 μm.

Once transplanted, suspensions of MSCs derived from MPC mesengenic differentiation (P2-MSCs, group *C* mice) generated non-vascularized xenogenic tissue composed almost exclusively of fat after 12 weeks (Figure 6A). Conversely, transplantation of "no sprouting control" 3D-spheroids (spP2-MSCs, group *D* mice) resulted in harder, more difficult-to-cut xenogenic tissue that appeared compact, acellular, and non-vascularized, lacking any organized collagen fiber network (Figure 6 B).

Histomorphometric analysis of sections from group *A* mice revealed a trend of increasing central median section (cmSC) total area, rising from 0.54 ± 0.08 mm² at 4 weeks to 1.53 ± 0.46 mm² at 12 weeks ($p < 0.05$, n=6). An inverse trend was observed in vessel density, which decreased to nearly zero by 12 weeks (1.8 ± 2.1 vessels/mm², n=6) compared to 4 weeks (239.1 ± 43.9 vessels/mm², $p < 0.005$, n=6), 6 weeks (196.6 ± 12.3 vessels/mm², $p < 0.001$, n=6), and 8 weeks (106.8 ± 2.3 vessels/mm², $p < 0.001$, n=6) (Figure 7A). In contrast, analysis of sections from group *B* mice showed that both the cmSC area (ranging from approximately 0.5 to 1.0 mm²) and vessel density (around 2 vessels/mm²)

 doi:10.20944/preprints202604.1955.v1

remained consistent across different sacrifice time points (Figure 7 B). No relevant violations of model assumptions were observed during statistical analysis.

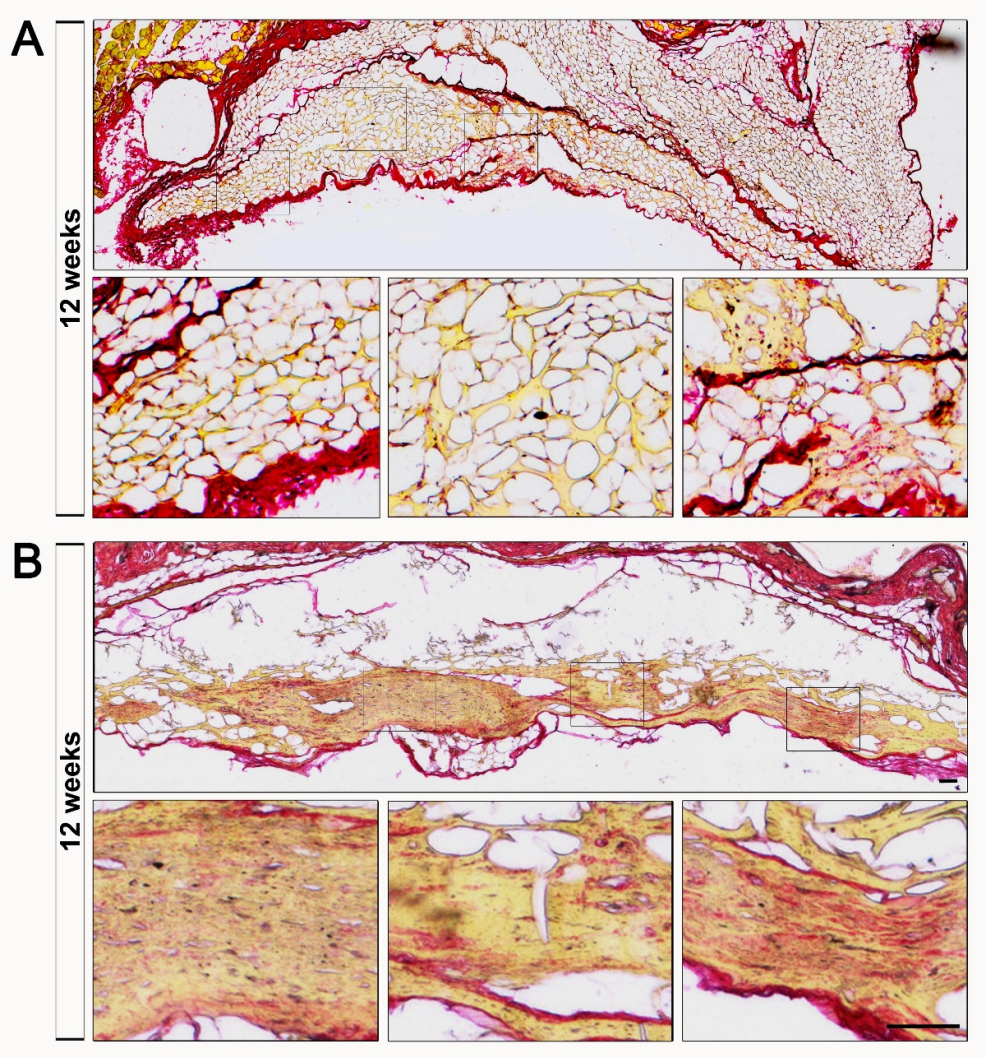

Figure 6. P*antachrome stain of the central median section +1 (cmSec+1) of excised nodules from groups C and D mice.* Nodules excised from control group mice implanted with MPC-derived MSC cell preparations exhibited markedly different xenogenic tissue organization after 12 weeks. (A) Transplantation of a suspension of P2-MSCs resulted in the formation of non-vascularized adipose tissue composed exclusively of large, mature adipocytes, with no associated collagen deposition. (B) Transplantation of the "no sprouting control" from group D mice produced compact, non-vascularized xenogenic tissue characterized by cutting-related grinding artifacts. Small areas of positive collagen staining (in red) were detected, although these were not organized into fibers. Scale bar = 250 μm.

Tissue composition analysis of group *A* sections confirmed a gradual thickening of the collagen fiber network, with a significant increase in the percentage of collagen relative area (%COLL, shown in purple false color in Figure 7 A) measured at 6 (24.8%), 8 (42.3%), and 12 (49.1%) weeks compared to 4 weeks (17.6%, $p < 0.0001$, n=6) after cell injection. However, after 8 weeks, the %COLL did not increase significantly. Sporadic lipid vacuoles, constituting less than 1% of the total area (%ADIPO, shown in yellow false color in Figure 8 A), were occasionally detected among the collected samples, with no significant variations. Analysis of group *B* sections at different sacrifice time points revealed no significant differences in %COLL, which ranged from approximately 25% to 50% of the total area,

 doi:10.20944/preprints202604.1955.v1

or in %ADIPO, which varied around 25% of the total area (Figure 8B). However, comparison between group *A* and group *B* at the same sacrifice time points showed a significantly higher %ADIPO in group B ($p < 0.05$, n=6) at all time points, while a significantly higher %COLL was detected only at 4 and 6 weeks ($p < 0.05$, data not shown). At 12 weeks post-cell injection, control group *C*, which received a suspension of P2-MSCs, consisted mostly of adipose tissue, with %ADIPO ranging from 50% to 70% of the total area ($p < 0.01$, n=6). No relevant violations of model assumptions were observed during statistical analysis. The tissue was not supported by an organized collagen network, as the AdipoBin binary image (in fuchsia false color) appeared significantly reduced and limited to the nodule's external surface. Similarly, no collagen fiber network was detected in group *D* mice, which received "no sprouting control" spheroids; approximately 95% of the total area was instead converted to the OstBin binary image (in blue false color in Figure 8C). Considering the disorganized architecture of these latest samples, further investigation into the genesis of such xenogenic tissue was deemed to have limited value. Therefore, no additional animals from groups *C* and *D* were sacrificed at different time points.

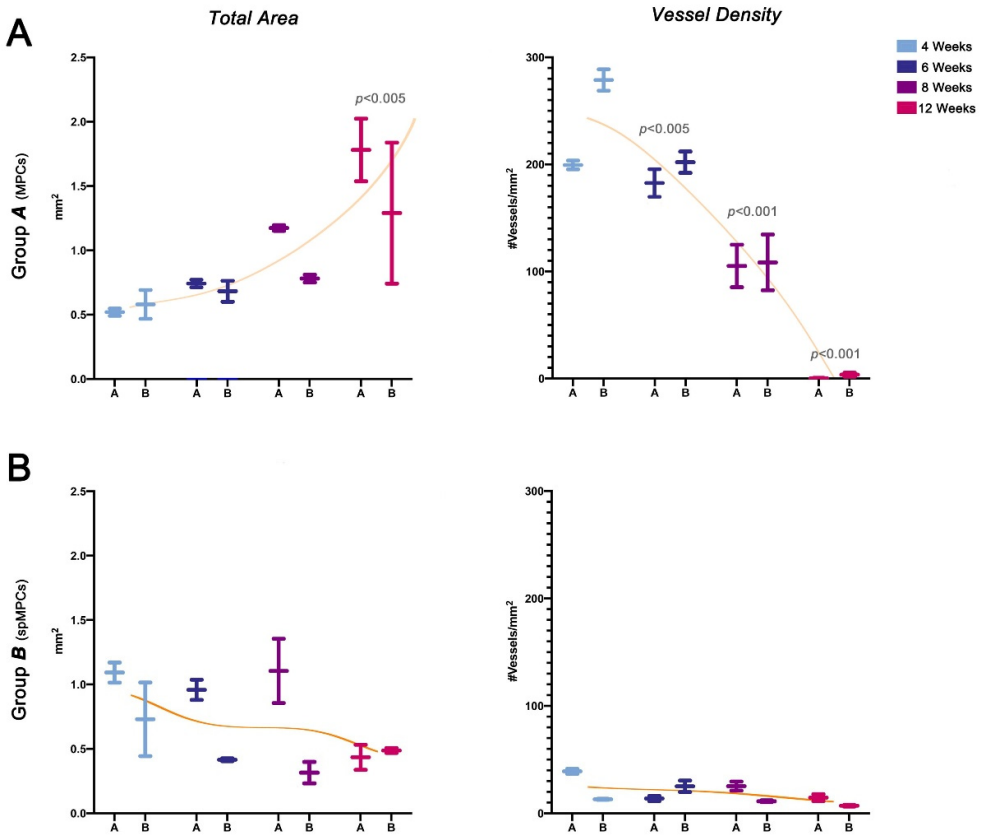

Figure 7. *Histomorphometric analysis: total area and vessel density*. (A) Evaluation of cmSec total area in Group *A* showed a significant 200% increase in mice sacrificed at 12 weeks compared to those at 4 and 6 weeks. Conversely, a significant and progressive reduction in vessel density was observed over time, resulting in nearly avascular nodules excised 12 weeks after cell injection. (B) Nodules from Group *B* mice exhibited high variability in cmSec total area (ranging from 0.5 to 1.0 mm²) with no significant differences over time. Vascularization detected at 4 weeks was consistently lower than in group *A* samples, with only a few dozen vessels per μm² compared to hundreds. No significant changes in tissue vascularization were observed over time in mice receiving sprouted MPCs.

 doi:10.20944/preprints202604.1955.v1

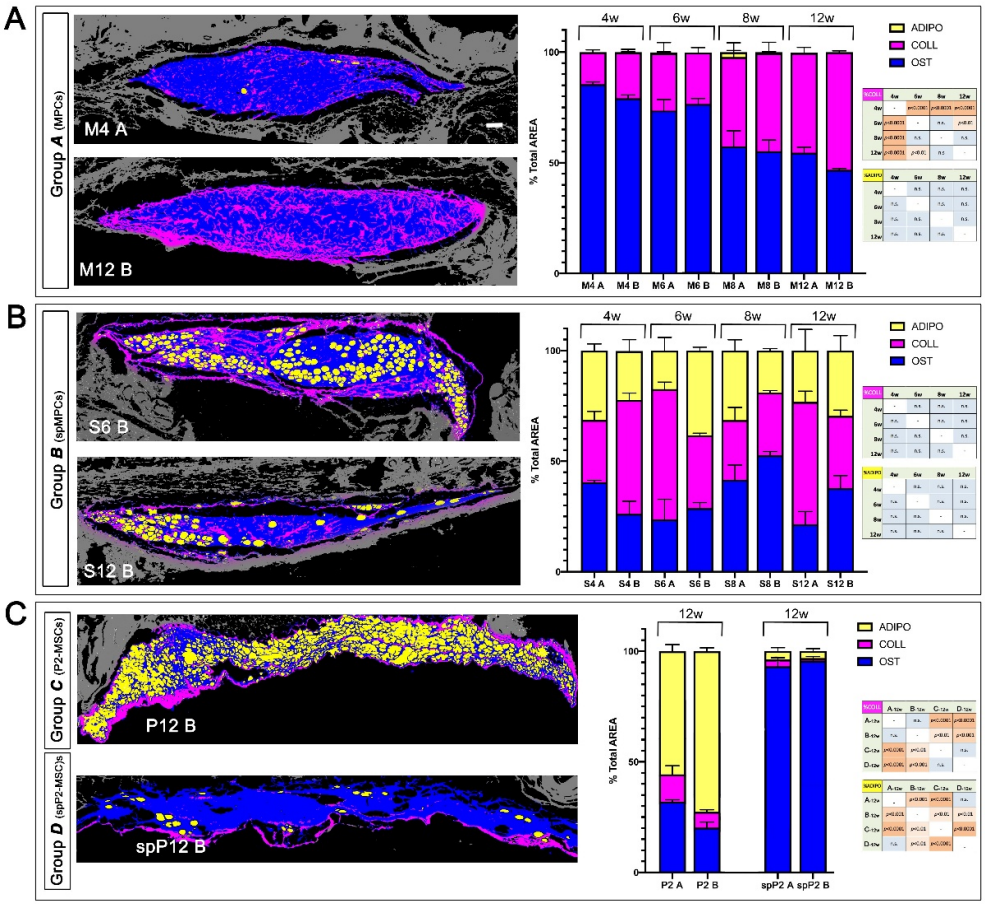

Figure 8. *Histomorphometric analysis: tissue composition.* (A) Nodules excised from mice receiving a suspension of MPCs (Group *A*) showed an increasing percentage of area stained scarlet red (represented in fuchsia false color, COLL) as the time to sacrifice increased, with approximately 50% collagen area measured after 12 weeks. Adipose tissue (depicted in yellow false color, ADIPO) was not detected, except for a few sporadic lipid vacuoles. (B) Tissue analysis of nodules excised from mice transplanted with MPC-derived sprouted spheroids (group *B*) revealed a more balanced composition among adipose, collagen, and osteoid-like (shown in blue false color, OST) area percentages, with no significant differences observed among the sample groups. (C) Nodules excised from mice transplanted with a suspension of P2-MSCs and sacrificed after 12 weeks were composed mostly of adipose tissue, ranging from 50% to 70% of the total area. Scale bar = 250 μm.

4. Discussion

Since their initial identification and characterization, MPCs have been reported to express *Oct-4* and *Nanog*, but not *Sox2*. These are master transcription factors involved in maintaining the undifferentiated state and self-renewal of embryonic stem cells (ESCs) and induced pluripotent stem cells (iPSCs) [1]. Further investigations revealed a distinctive pluripotency-associated molecular signature in MPCs, leading to the hypothesis that their multipotency may be sustained by the activity of both the *Oct-4*/*Oct-4* homodimer and the *Oct-4*/*Sox15* heterodimer within a regulatory circuit that also involves *Nanog* and *Sall4* [9]. This hypothesis is partially supported by the consistent expression of target genes such as *SSP1*, which encodes *osteopontin* and has recently been demonstrated to be a target of the *Oct-4*/*Oct-4* dimer [17]. Additionally, data show that *Oct-4* can bind *Sox2* or *Sox15* with comparable affinity [18] and directly activate key pluripotency genes such as *NANOG* [19] and *FBX15* [20], both of which are highly expressed in MPCs [9]. Taken together, all these data suggest that MPCs may retain embryonic-like cell plasticity in adults. Recently, it has been hypothesized that MPCs represent the cell identity toward which the de-differentiation process reprograms circulating

 doi:10.20944/preprints202604.1955.v1

monocytes and macrophages, enabling them to transdifferentiate into osteogenic, adipogenic, chondrogenic, and vasculogenic cells [21]. Although MPCs are isolated as quiescent and Ki-67-negative cells [1], concerns remain regarding their tumorigenic potential once transplanted. Currently, the World Health Organization (WHO) Technical Report Series (TRS) No.878 Annex 3 provides the only international guideline addressing tumorigenicity tests in the production of biological medicinal products [10]. However, the in vivo tumorigenicity test described in WHO TRS 878 is designed for viable animal cells used as cell substrates in the manufacture of biological products, not for cells intended for direct transplantation into patients as part of cell therapy. Furthermore, WHO guidelines recommend administering 10^7 cells to ten nude mice to achieve the sensitivity required to detect trace amounts of tumorigenic cellular impurities in human cell-based medicinal products (CBMPs). Implementing this recommendation requires producing at least 10^8 cells solely for tumorigenicity testing, which is impractical for somatic or progenitor cell-based CBMPs. Consequently, to date, no suitable tumorigenicity test has been established for CBMPs in general, particularly for slow-growing or non-proliferating cells such as MPCs [22].

Here, we present data obtained using a model partially compliant with WHO recommendations for testing tumorigenicity [10], demonstrating that freshly isolated MPCs and MPC-derived cell products, at a cell dose considered clinically feasible based on the quantity of starting material, are unable to form tumors in athymic nude mice. Nonetheless, the use of a commercialized basement membrane matrix, derived from Engelbreth-Holm-Swarm mouse sarcoma cells [23], as injection vehicle has been reported to facilitate human tumor xenograft growth in rodents [24] and significantly increase the sensitivity of tumorigenic tests [25]. Thus, although the MPC dose was ten times lower than the WHO recommendation, it is reasonable to hypothesize that the test sensitivity could be sufficiently high due to the reported 30-fold increase resulting from the use of basement membrane matrix as the injection vehicle, where the highest cell dose tested was 10^6 per injection, comparable to the cell dose applied in our experiments. However, it is important to note that the test described here is intended to verify whether MPCs are intrinsically tumorigenic, as they constitutively express pluripotency-associated genes, and not to guarantee the “safety” of the cell product. [26].

Interestingly, histological evaluation of xenograft explanted nodules revealed significant microscopic differences depending on the transplanted cell product, an observation that warrants particular attention beyond the scope of tumorigenicity testing. Overall, histomorphometric analysis indicates that MPC-containing cell products have the capacity to dynamically form organized tissues within a poorly vascularized microenvironment, such as the subcutaneous space. In contrast, MSC-containing products produced uniformly amorphous nodules, likely resulting from cell degeneration. Specifically, nodule formation following MPC injection appears to be regulated by two distinct and opposing dynamic processes: new vessel formation and collagen network stabilization. During the early phase, within four weeks post-injection, intense vasculogenic activity generated more than 200 CD34-positive, nestin-positive microvessels per cm^2. The morphology of these newly formed vessels closely resembles that of endosteal arterioles (EA) described in mice [27] and human bone marrow [28,29]. At this stage, collagen deposition was limited to a few fibrils, occupying less than 20% of the total area. With the increased deposition and stabilization of a thicker collagen fibre network, vessel density significantly decreased to only a few vessels per cm^2. This preliminary observation suggests a compelling hypothesis: transient vascularization occurs during the initial phase of cartilage and bone repair, serving a fundamental role by supplying the newly formed tissue with adequate nutrients and oxygen. Subsequently, as the repair tissue matures, it reverts to an avascular or poorly vascularized state characteristic of healthy bone or articular cartilage, as noted in previous studies [30,31]. Therefore, the combined mesengenic and vasculogenic potential within a unique progenitor cell population makes MPCs particularly promising for musculoskeletal regeneration in such hostile microenvironments, which may present biological challenges to cell therapy approaches. Indeed, this may also explain the disappointing results observed in the application of MSCs in cell therapy [32], supporting the hypothesis that the clinical efficacy of stem

 doi:10.20944/preprints202604.1955.v1

cells could be limited by the harsh microenvironment, characterized by oxygen and nutrient deprivation resulting from the degenerative process, into which these cells are transplanted [33]. In contrast, the aforementioned progression of events following MPC transplantation suggests a potential mechanism to overcome these limitations. Notably, very similar kinetic and tissue morphology have been detected in portions of the heterogeneous nodules obtained by injecting sprouted 3D-spheroids. This could be explained by considering the methods applied to induce endothelial differentiation, which possibly generate a stimulus gradient from the outer to the inner regions of the spheroids, an extensively investigated effect during their in vitro fabrication [34,35]. Therefore, the cell fate in the central regions would be similar to unstimulated MPCs, also resulting in an arteriolar vasculature. Meanwhile, cells close to the spheroid surface, receiving the in vitro endothelial-differentiating stimulus, would support the neo-formation of a nestin-negative sinusoidal vasculature in vivo, lacking stabilizing perivascular cells and in close contact with large, mature adipocytes [36]. Although the human origin of the newly formed microvasculature detected in the xenografts requires further investigation, these corollary observations on dynamic xenograft tissue formation, whether MPCs support vasculogenesis directly through differentiation or indirectly by stimulating angiogenesis in the surrounding vasculature, raise expectations regarding the promising clinical value of MPC transplantation compared to current MSC-based cell therapy approaches.

5. Conclusions

All these data further confirm the potential of MPC in musculoskeletal tissue regeneration. Although further investigations in relevant animal models of musculoskeletal tissue degeneration are needed to definitely evaluate the efficacy of MPC in regenerating medicine, however excluding the intrinsic tumorigenic potential represents a fundamental step toward the definition of MPC-based medicinal products. However, it is urgent to establish reasonable recommendations for testing the tumorigenicity of somatic cells intended for transplantation as CBMPs, considering the inherent risks associated with applying these biological products. This risk is fundamentally different from that of transplanting trace amounts of cells that are constitutively pluripotent and teratogenic, such as iPSC-derived products.

Supplementary Materials: The following supporting information can be downloaded at: Preprints.org.

Author Contributions: Conceptualization, SP and GB; methodology, MM, PO, AP, EP and SB.; formal analysis, SP and GB; resources and sample collection, PDP; data curation, SP, AP and GB; writing—original draft preparation, SP.; writing—review and editing, AP, BG. All authors have read and agreed to the published version of the manuscript.".

Funding: This research received no external funding.

Institutional Review Board Statement: The human bone marrow sample collection was conducted in accordance with the Declaration of Helsinki, and approved by the local "CESF" ethics committee of the "*Azienda Ospedaliero-Universitaria Pisana*" (protocol code 27880/2016). The animal study protocol was approved by the Academic Organization Responsible for Animal Welfare [*Organismo Preposto per il Benessere Animale (OPBA)*] of the University of Pisa, following the Italian law D.lgs. 26/2014, and by the Italian Ministry of Health (Authorization No. 609/2017-PR, July 28th 2017).

Informed Consent Statement: "Informed consent was obtained from all subjects involved in the study.".

Data Availability Statement: The original contributions presented in this study are included in the article/supplementary material. Further inquiries can be directed to the corresponding author.

Acknowledgments: The authors would like to thank Francesca M. Panvini for her insightful contributions to the conceptualization of this work and for her valuable suggestions during the preparation of the manuscript. The

 doi:10.20944/preprints202604.1955.v1

authors would also like to thank Andrew Mearns Spragg for his valuable suggestions and for revising the style and grammar of the manuscript.

Conflicts of Interest: The authors declare no conflicts of interest.

Abbreviations

The following abbreviations are used in this manuscript:

MPC	Mesangiogenic Progenitor Cell
MSC	Mesenchymal Stromal Cell
CBMP	Cell-based Medicinal product
BM	Bone Marrow
hBM-MNC	Human Bone Marrow Mononuclear Cell
hPSC	Human Pluripotent stem cell
SE	Standard Error
3D	Three dimensions
WHO	World Health Organization
OCT-4	Octamer-binding transcription factor 4
SOX15	SRY-box transcription factor 15

References

1. Petrini, M.; Pacini, S.; Trombi, L.; Fazzi, R.; Montali, M.; Ikehara, S.; Abraham, N.G. Identification and purification of mesodermal progenitor cells from human adult bone marrow.. Stem Cells Dev 2009, 18, 857–66.
2. Montali, M.; Barachini, S.; Pacini, S.; Panvini, F.M.; Petrini, M. Isolating Mesangiogenic Progenitor Cells (MPCs) from Human Bone Marrow.. J Vis Exp 2016.
3. Fazzi, R.; Pacini, S.; Carnicelli, V.; Trombi, L.; Montali, M.; Lazzarini, E.; Petrini, M. Mesodermal progenitor cells (MPCs) differentiate into mesenchymal stromal cells (MSCs) by activation of Wnt5/calmodulin signalling pathway.. PLoS One 2011, 6, e25600.
4. Montali, M.; Panvini, F.M.; Barachini, S.; Ronca, F.; Carnicelli, V.; Mazzoni, S.; Petrini, I.; Pacini, S. Human adult mesangiogenic progenitor cells reveal an early angiogenic potential, which is lost after mesengenic differentiation.. Stem Cell Res Ther 2017, 8, 106.
5. Pacini, S.; Barachini, S.; Montali, M.; Carnicelli, V.; Fazzi, R.; Parchi, P.; Petrini, M. Mesangiogenic Progenitor Cells Derived from One Novel CD64(bright)CD31(bright)CD14(neg) Population in Human Adult Bone Marrow.. Stem Cells Dev 2016, 25, 661–73.
6. Pacini, S. Deterministic and stochastic approaches in the clinical application of mesenchymal stromal cells (MSCs).. Front Cell Dev Biol 2014, 2, 50.
7. Perez, J.R.; Kouroupis, D.; Li, D.J.; Best, T.M.; Kaplan, L.; Correa, D. Tissue Engineering and Cell-Based Therapies for Fractures and Bone Defects.. Front Bioeng Biotechnol 2018, 6, 105.
8. Ilic, D.; Ogilvie, C. Pluripotent Stem Cells in Clinical Setting-New Developments and Overview of Current Status.. Stem Cells 2022, 40, 791–801.
9. Pacini, S.; Carnicelli, V.; Trombi, L.; Montali, M.; Fazzi, R.; Lazzarini, E.; Giannotti, S.; Petrini, M. Constitutive expression of pluripotency-associated genes in mesodermal progenitor cells (MPCs).. PLoS One 2010, 5, e9861.
10. World Health Organizzation, Recommendations for the evaluation of animal cell cultures as substrates for the manufacture of biological medicinal products and for the characterization of cell banks; Annex 3, 2013;
11. Sato, Y.; Bando, H.; Di, P.M.; Gowing, G.; Herberts, C.; Jackman, S.; Leoni, G.; Libertini, S.; MacLachlan, T.; McBlane, J.W.; et al. Tumorigenicity assessment of cell therapy products: The need for global consensus and points to consider.. Cytotherapy 2019, 21, 1095–1111.
12. Delgado, J.A.; Guillén-Grima, F.; Moreno, C.; Panizo, C.; Pérez-Robles, C.; Mata, J.J.; Moreno, L.; Arana, P.; Chocarro, S.; Merino, J. A simple flow-cytometry method to evaluate peripheral blood contamination of bone marrow aspirates.. J Immunol Methods 2017, 442, 54–58.

 doi:10.20944/preprints202604.1955.v1

13. Doello, K. A new pentachrome method for the simultaneous staining of collagen and sulfated mucopolysaccharides. Yale J Biol Med 2014, 87, 341–7.
14. IARC/WHO. Classification of Tumours Editorial Board. WHO Classification of Tumours Online. 5th Edition. International Agency for Research on Cancer; 2019–2026
15. Leung S.C.Y.; Nielsen T.O.; Zabaglo L.A.; Arun I.; Badve S.S.; Bane A.L.; Bartlett J.M.S.; Borgquist S.; Chang M.C.; Dodson A.; et al. Analytical validation of a standardised scoring protocol for Ki67 immunohistochemistry on breast cancer excision whole sections: an international multicentre collaboration.. Histopathology. 2019, 75, 225-235.
16. Schmitz F.; Voigtländer H.; Strauss D.; Schlemmer H.P.; Kauczor H.U.; Jang H.; Sedaghat S. Differentiating low- and high-proliferative soft tissue sarcomas using conventional imaging features and radiomics on MRI. BMC Cancer. 2024, 30, 24(1), 1589.
17. Botquin, V.; Hess, H.; Fuhrmann, G.; Anastassiadis, C.; Gross, M.K.; Vriend, G.; Schöler, H.R. New POU dimer configuration mediates antagonistic control of an osteopontin preimplantation enhancer by Oct-4 and Sox-2.. Genes Dev 1998, 12, 2073–90.
18. Ng, C.K.; Li, N.X.; Chee, S.; Prabhakar, S.; Kolatkar, P.R.; Jauch, R. Deciphering the Sox-Oct partner code by quantitative cooperativity measurements.. Nucleic Acids Res 2012, 40, 4933–41.
19. Choi, E.B.; Vodnala, M.; Saini, P.; Anugula, S.; Zerbato, M.; Ho, J.J.; Wang, J.; Ho, S.S.J.; Yoon, J.; Roels, M.; et al. Transcription factor SOX15 regulates stem cell pluripotency and promotes neural fate during differentiation by activating the neurogenic gene Hes5.. J Biol Chem 2023, 299, 102996.
20. Tokuzawa, Y.; Kaiho, E.; Maruyama, M.; Takahashi, K.; Mitsui, K.; Maeda, M.; Niwa, H.; Yamanaka, S. Fbx15 is a novel target of Oct3/4 but is dispensable for embryonic stem cell self-renewal and mouse development.. Mol Cell Biol 2003, 23, 2699–708.
21. Pacini, S. Mesangiogenic progenitor cells: a mesengenic and vasculogenic branch of hemopoiesis? A story of neglected plasticity.. Front Cell Dev Biol 2025, 13, 1513440.
22. Dou D.; Lu J.; Dou J.; Huo Y.; Gong X.; Zhang X.; Chen X. Global regulatory considerations and practices for tumorigenicity evaluation of cell-based therapy.. Regul Toxicol Pharmacol. 2025, 156, 105769
23. Kleinman H.K.; McGarvey M.L.; Hassell J.R.; Star V.L.; Cannon F.B.; Laurie G.W.; Martin G.R. Basement membrane complexes with biological activity.. Biochemistry. 1986, 28, 25(2),312-8
24. Fridman R.; Giaccone G.; Kanemoto T.; Martin G.R.; Gazdar A.F.; Mulshine J.L. Reconstituted basement membrane (matrigel) and laminin can enhance the tumorigenicity and the drug resistance of small cell lung cancer cell lines.. Proc Natl Acad Sci U S A. 1990, 87(17), 6698-702.
25. Kusakawa S.; Machida K.; Yasuda S.; Takada N.; Kuroda T.; Sawada R.; Okura H.; Tsutsumi H.; Kawamata S.; Sato Y. Characterization of *in vivo* tumorigenicity tests using severe immunodeficient NOD/Shi-scid IL2Rγ^{null} mice for detection of tumorigenic cellular impurities in human cell-processed therapeutic products.. Regen Ther. 2015, 19, 1, 30-37.
26. Wang Z. Assessing Tumorigenicity in Stem Cell-Derived Therapeutic Products: A Critical Step in Safeguarding Regenerative Medicine.. Bioengineering (Basel). 2023, 19, 10(7), 857.
27. Itkin T.; Gur-Cohen S.; Spencer J.A.; Schajnovitz A.; Ramasamy S.K.; Kusumbe A.P.; Ledergor G.; Jung Y.; Milo I.; Poulos M.G.; et al. Distinct bone marrow blood vessels differentially regulate haematopoiesis.. Nature. 2016, 21, 532(7599), 323-8.
28. Panvini, F.M.; Pacini, S.; Montali, M.; Barachini, S.; Mazzoni, S.; Morganti, R.; Ciancia, E.M.; Carnicelli, V.; Petrini, M. High NESTIN Expression Marks the Endosteal Capillary Network in Human Bone Marrow.. Front Cell Dev Biol 2020, 8, 596452.
29. Boueya I.L.; Sandhow L.; Albuquerque J.R.P.; Znaidi R.; Passaro D. Endothelial heterogeneity in bone marrow: insights across development, adult life and leukemia.. Leukemia. 2025, 39(1), 8-24
30. Rao, R.R.; Stegemann, J.P. Cell-based approaches to the engineering of vascularized bone tissue.. Cytotherapy 2013, 15, 1309–
31. Takebe, T.; Kobayashi, S.; Suzuki, H.; Mizuno, M.; Chang, Y.M.; Yoshizawa, E.; Kimura, M.; Hori, A.; Asano, J.; Maegawa, J.; et al. Transient vascularization of transplanted human adult-derived progenitors promotes self-organizing cartilage.. J Clin Invest 2014, 124, 4325–34.

 doi:10.20944/preprints202604.1955.v1

32. Cong B.; Zhang F.H.; Zhang H.G. Stem cell-based cartilage regeneration: Biological strategies, engineering innovations, and clinical translation.. World J Stem Cells. 2025, 26, 17(9), 108523
33. Chu G.; Zhang W.; Han F.; Li K.; Liu C.; Wei Q.; Wang H.; Liu Y.; Han F.; Li B. The role of microenvironment in stem cell-based regeneration of intervertebral disc.. Front Bioeng Biotechnol. 2022, 9, 10, 968862
34. Decarli, M.C.; Amaral, R.; Santos, D.P.dos; Tofani, L.B.; Katayama, E.; Rezende, R.A.; Silva, J.V.L.da; Swiech, K.; Suazo, C.A.T.; Mota, C.; et al. Cell spheroids as a versatile research platform: formation mechanisms, high throughput production, characterization and applications. Biofabrication 2021, 13.
35. Vakhrushev, I.V.; Nezhurina, E.K.; Karalkin, P.A.; Tsvetkova, A.V.; Sergeeva, N.S.; Majouga, A.G.; Yarygin, K.N. Heterotypic Multicellular Spheroids as Experimental and Preclinical Models of Sprouting Angiogenesis.. Biology (Basel) 2021, 11.
36. Xu, Z.; Kusumbe, A.P.; Cai, H.; Wan, Q.; Chen, J. Type H blood vessels in coupling angiogenesis-osteogenesis and its application in bone tissue engineering. Journal of Biomedical Materials Research Part B: Applied Biomaterials 2023, 111.